Pergamon

Geochimica et Cosmochimica Acta, Vol. 62, No. 12, pp. 2143–2154, 1998

0016-7037/98 $19.00 + .00

PII S0016-7037(98)00142-2

Graphite pseudomorphs after diamond? A carbon isotope and spectroscopic study of graphite cuboids from the Maksyutov Complex, south Ural Mountains, Russia

MARY L. LEECH and W. G. ERNST

Department of Geological and Environmental Sciences, Stanford University, Stanford, California 94305-2115, USA

(*Received November* 12, 1997; *accepted in revised form March* 26, 1998)

ABSTRACT—Unusual cuboid graphite aggregates (up to 13 mm edge length) from the eclogitic gneiss unit of the Maksyutov Complex deflect a foliation defined by groundmass graphite and phengite, and pressure shadows have developed around these blocky aggregates. Carbon isotope ratios, $\delta^{13}C/^{12}C$, for the cuboid graphite range from about −24 to −42‰, demonstrating that these rocks have retained an original biogenic carbon signature. X-ray diffraction, laser Raman spectroscopy, infrared spectroscopy, and transmission electron microscopy indicate that graphite is well-crystallized with minor defects; no relict organic compounds were detected. Comparisons of these cuboid aggregates with thin sections and scanning electron microscope images of proven graphitized diamonds from the Beni Bousera peridotite massif show that Maksyutov graphite is similar. Laboratory experiments by other workers on graphite demonstrate that this intriguing morphology could not be the result of deformation, because graphite returns to its original shape and size on stress release. Existing experiments on diamond graphitization do not adequately replicate the conditions of natural rocks being exhumed from subduction zones characterized by ultrahigh pressures, and thus cannot be applied with confidence to the Maksyutov Complex. Our spectroscopic and microscopic studies suggest that these cuboid aggregates probably are diamond pseudomorphs. *Copyright © 1998 Elsevier Science Ltd*

1. INTRODUCTION

Graphite pseudomorphs after diamond have been recognized in the Beni Bousera peridotite massif in northern Morocco and the Ronda peridotite massif in southern Spain (e.g., Pearson et al., 1989; Davies et al., 1993). Scanning electron microscope (SEM) imagery of graphite from these massifs revealed octahedral and cubic faces with corresponding depressions within graphite and showed that thin coatings of differently-oriented graphite surround the pseudomorphs.

Thus far, only a few crustal terranes subjected to ultrahigh pressure (UHP) have been recognized worldwide: the Kokchetav Massif in northern Kazakhstan, the Sulu-Dabie belt in east-central China, the Dora Maira Massif in the Italian Alps, and the Western Gneiss Region in coastal Norway are examples of well-studied UHP continental terranes with confirmed coesite, coesite pseudomorphs, and, in the case of the Kokchetav occurrence, diamond. Rare occurrences of microdiamond inclusions have also been described from the Dabie Shan (Xu et al., 1992; Okay, 1993) and from the Western Gneiss region (Dobrzhinetskaya et al., 1995). Reports of coesite pseudomorphs in the eclogitic unit of the Maksyutov Complex (Chesnokov and Popov, 1965; Dobretsov and Dobretsova, 1988) suggest that these rocks, too, may have been metamorphosed at ultrahigh pressures. Although thermobarometric calculations have demonstrated minimum conditions of about 600°C, 1.5 GPa for the Maksyutov Complex (Beane et al., 1995; Lennykh et al., 1995; Dobretsov et al., 1996; Beane, 1997), cuboid graphite aggregates from host mica schist support the earlier suggestion of UHP metamorphism proposed by Chesnokov and Popov (1965) and Dobretsov and Dobretsova (1988).

Reports of coesite have not been independently confirmed, but if the cuboid graphite is pseudomorphic after diamond, it would indicate even higher pressures than previously thought. Graphite aggregates pseudomorphic after diamond may occur unrecognized elsewhere in continental collision zones; if our speculations about the Maksyutov paragenesis are correct, this example could encourage further study of carbonaceous matter.

2. GEOLOGIC SETTING

The Maksyutov Complex trends north-south in the south Ural Mountains of central Russia (Fig. 1). The complex consists of two main units tectonically juxtaposed in this continental collision suture zone (Zonenshain et al., 1990): an eclogite-bearing gneiss, called Unit #1; and a meta-ophiolite, termed Unit #2. Unit #1 contains boudins of eclogite, layers of eclogitic gneiss, and rare ultramafic bodies within host metasedimentary mica schist and quartzite; Unit #2 consists of lenses of serpentinite melange and blocks of metasomatic rock (~rodingite), metabasalt, and marble within mica schist and graphite quartzite host rock (Fig. 2). Unit #1 protoliths are Middle to Late Proterozoic; Unit #2 is Late Proterozoic with blocks of Ordovician to Silurian marble (Dobretsov et al., 1996). Unit #2, considered to tectonically overlie Unit #2 (Lennykh et al., 1995), was probably thrust over Unit #1 after the Middle Devonian HP-UHP metamorphic event that affected Unit #1 and the Early Carboniferous retrograde blueschist- to high-pressure greenschist-facies metamorphism that affected Unit #2 (Matte et al., 1993; Beane, 1997; Beane et al., 1995). Both units were overprinted by a late, low-pressure, greenschist-facies metamorphism and subsequently folded together about NE-SW trending axes.

Fe-Mg exchange geothermometry calculated for garnet and clinopyroxene (after Powell, 1985) yields an equilibrium temperature ranging from 594 to 637°C. Minimum pressure estimates using the jadeite component of clinopyroxene (after

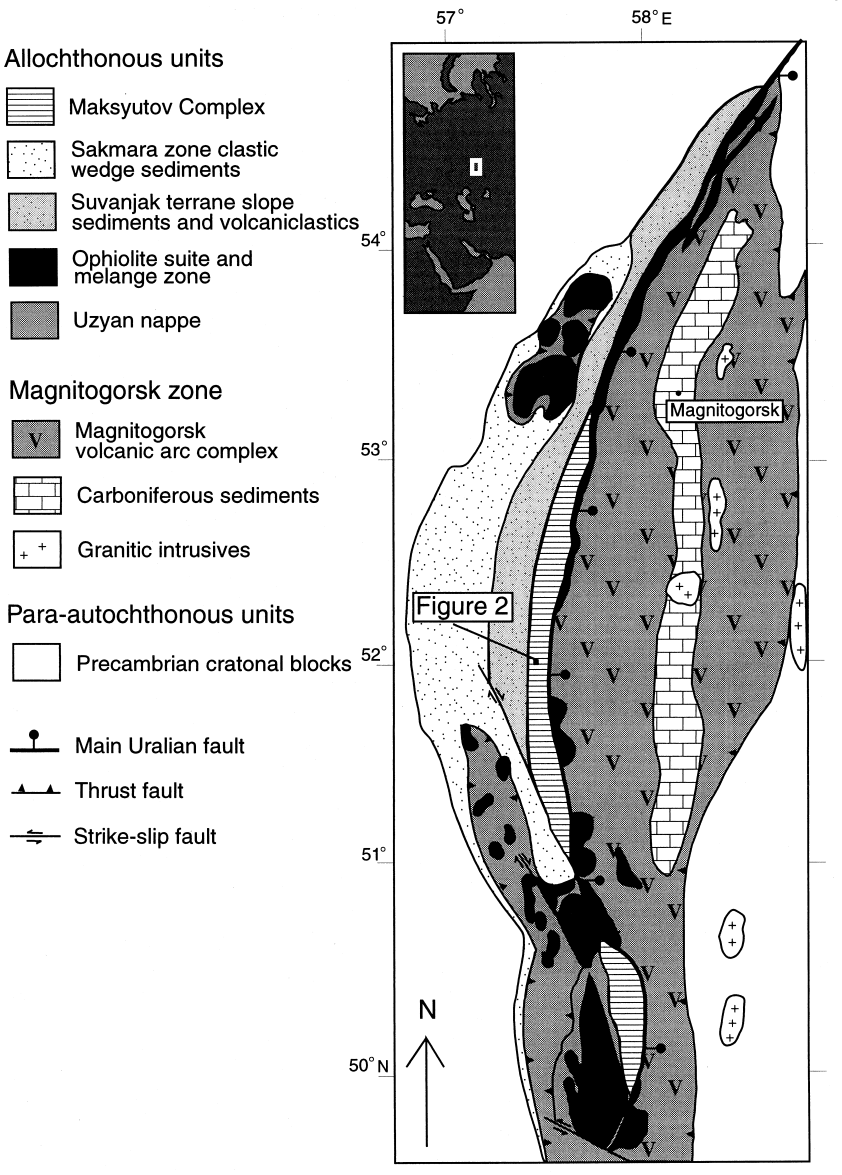

Fig. 1. Tectonic map of the south Ural Mountains, Russia, the collisional zone between the East European platform and the Siberian craton. The inset map shows the location of the figure. After Beane et al. (1995).

Holland, 1980) range from 1.5 to 1.7 GPa (Beane et al., 1995; Lennykh et al., 1995; this study), but may be as high as 2.7 GPa if coesite pseudomorphs described in eclogite (Chesnokov and Popov, 1965) and jadeite quartzite (Dobretsov and Dobretsova, 1988) are present (Bohlen and Boettcher, 1982). Thermobarometric estimates may represent annealing during exhumation in which minerals reequilibrated at lower P-T conditions, leaving little evidence of UHP metamorphism (Fig. 3).

3. CUBOID GRAPHITE, PSEUDOMORPHS AFTER DIAMOND?

3.1. Petrography

Graphite-phengite schist (sample M-16-94) from near the former village of Karayanova contains 40% phengite, 38% graphite, 19% quartz, 1% rutile, <1% zircon, and <1% iron oxide minerals. A single cleavage is defined by oriented phengite and graphite flakes. The flakes wrap around large, subangular, blocky graphite aggregates; pressure shadows containing quartz and coarse-grained phengite have developed around the aggregates, suggesting that during deformation, the aggregates behaved as coherent, rigid blocks within a more ductile matrix (Fig. 4a). Aligned inclusions of phengite and rutile in the graphite aggregates are subparallel to the foliation. Graphite aggregates have an angular to subrounded cross-sectional morphology (Fig. 4b); this is significant because these aggregates may be pseudomorphs after diamond indicating ultrahigh-pressure metamorphism at a minimum pressure of about 3.2 GPa (Kennedy and Kennedy, 1976).

Graphite is abundant throughout the Maksyutov Complex, with volumetric modes in the mica schists locally ranging up to

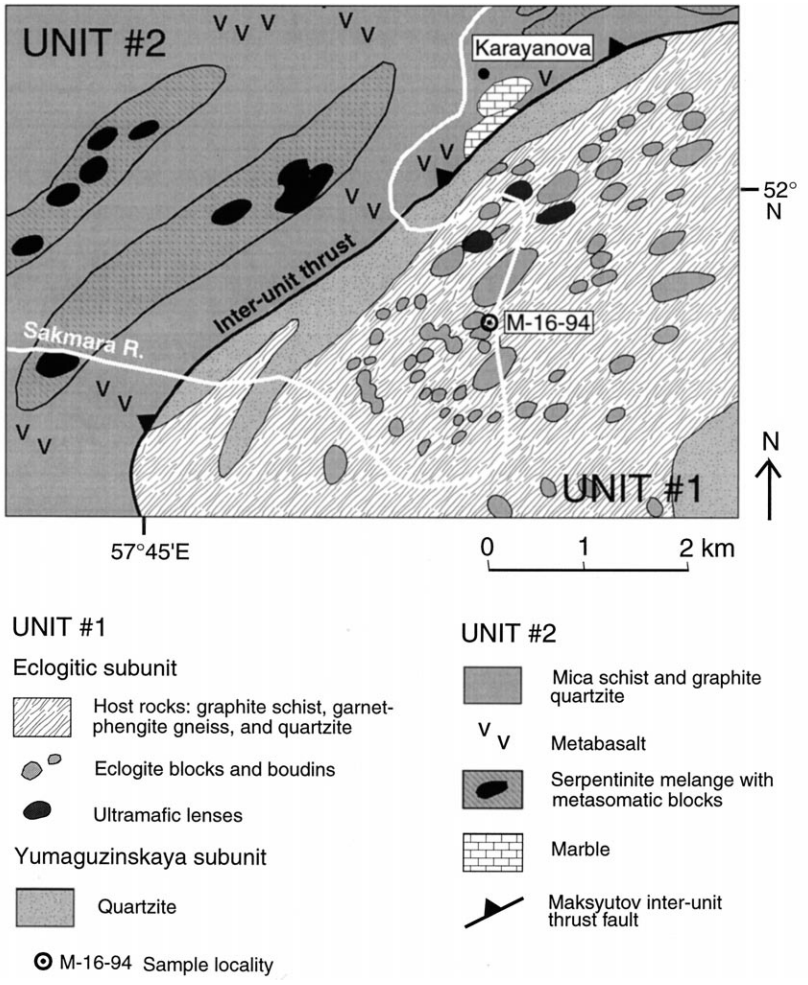

Fig. 2. Geologic map of the Maksyutov Complex showing exposure of Units #1 and #2 along the Sakmara River near Karayanova (see Fig. 1). Sample M-16-94 indicates where cuboid aggregates occur. After Lennykh et al. (1995).

38% graphite. Disseminated tabular graphite occurs parallel to the dominant foliation in quartzites of both Units #1 and #2 and in metasomatic rocks of Unit #2. Cuboid graphite aggregates (most <5 mm long, but up to 13×10 mm), made up of flakes ranging in size from about 4 to 100 μm, are found in mica schist near Karayanova, and occur with graphite flakes aligned in the foliation. Scanning electron microscope images show cubic forms of the graphite aggregates (Fig. 5). Graphite is also found as inclusions in garnet in eclogitic gneisses near Antingan village.

3.2. Graphite Deformation

Are these cuboid graphite aggregates a result of a specific deformation mechanism acting on graphite? Indeed, how does graphite deform under the P-T conditions and differential stress these rocks experienced? Edmond and Paterson (1971) described stress-strain experiments for graphite samples (10×20 mm) under confining pressures up to 0.8 or 1.0 GPa and room temperature. Under these conditions, they found that graphite specimens returned almost to their original dimensions when both the differential stress and confining pressure were released, even after 20% shortening at 0.4 GPa; other samples were shortened 20% under confining pressures of 0.2–0.8 GPa and gave similar recoveries. Later experiments by Edmond and Paterson (1972) showed that, in addition to an almost complete recovery of volume, the initial shape of the graphite was retained as well, with most of the recovery occurring below 0.05 GPa; graphite specimens appeared to be undeformed.

Kretz (1996) described graphite in high-grade marble ($T = 650–700°C$; $P = 0.65–0.70$ GPa) occurring as both undeformed and deformed tabular grains and suggested that the deformational behavior of graphite is similar to that of biotite. Graphite deforms by cleavage separation, kink-band formation, and folding; breaking across the (0001) basal plane of strong carbon bonds occurred only in mylonitic marble where strain rates were very high.

3.3. Graphitization of Organic Matter

Is this poorly crystallized graphite? Graphitization of organic matter is primarily dependent on metamorphic temperature, but the process is facilitated at lower temperatures by shear strain in combination with elevated pressure (Landis, 1971; Teichmuller, 1987; Ross and Bustin, 1990; Ross et al., 1991). Temperatures and pressures suggested for the formation of true,

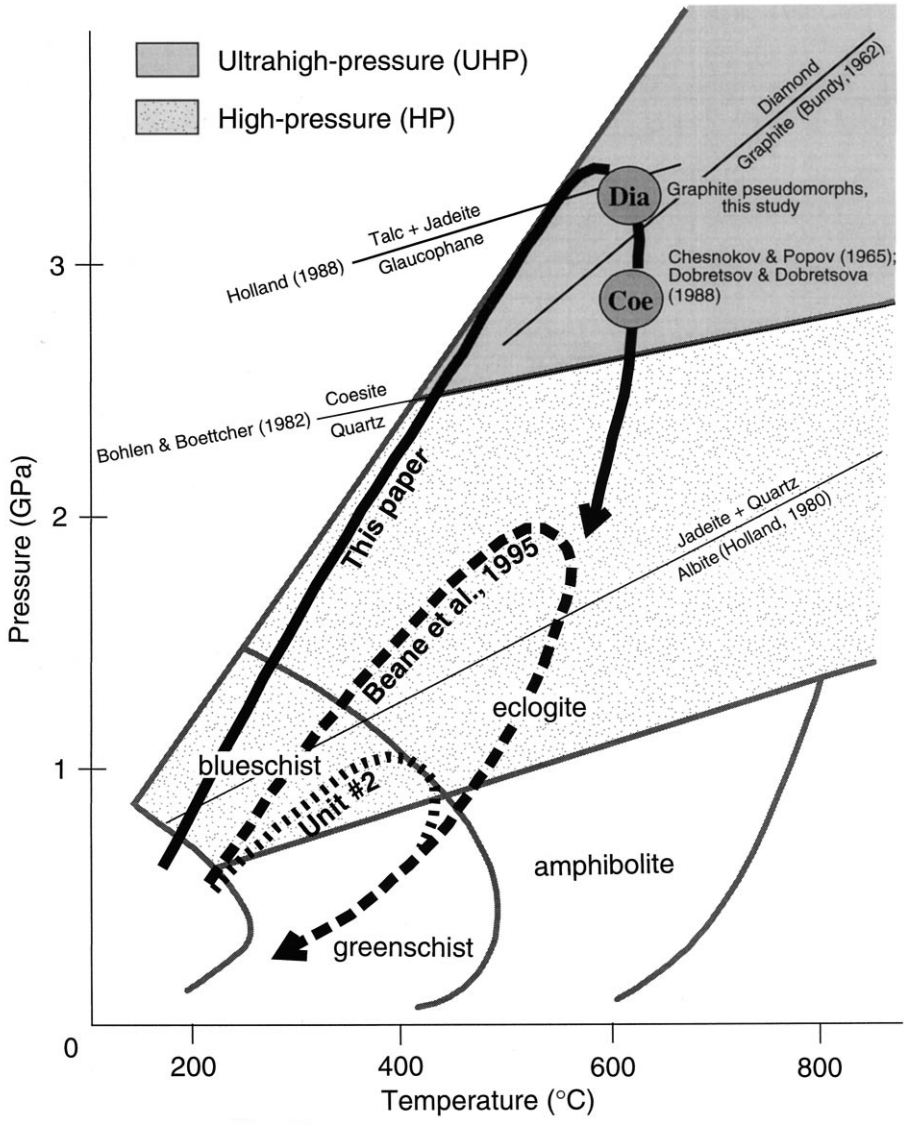

Fig. 3. Possible retrograde P-T paths for the Maksyutov Complex: The solid curve is based on Russian reports of coesite (Chesnokov and Popov, 1965; Dobretsov and Dobretsova, 1988) and possible graphite pseudomorphs after diamond (this study); a second possible P-T path is shown as a dashed curve in accordance with the thermobarometric calculations and petrographic studies conducted on eclogites and related rocks from Unit #1 (Beane et al., 1995). The dotted line shows the probable path for Unit #2 rocks. After Lennykh et al. (1995).

well-ordered graphite in nature range from about 350° to 700°C and from 0.2 to 0.6 GPa (Landis, 1971; Grew, 1974; Diessel et al., 1978; Tagiri and Oba, 1986).

Well-ordered graphite develops over a wide range of metamorphic conditions. Moderately high temperatures (sillimanite zone or amphibolite-facies) are required for near complete graphitization (Grew, 1974; Armstrong, 1982), although Buseck and Huang (1985) described well-ordered graphite in the chlorite zone (greenschist-facies). It is clear that increasing crystallinity is roughly proportional to metamorphic grade within a specific terrane, but not necessarily between terranes. However, higher pressures such as those calculated for the Maksyutov Complex may retard the graphitization process (Dalla Torre et al., 1996, 1997) even if metamorphic temperatures are above those required for complete graphitization at low pressures. With continued progressive metamorphism, the long-range order increases, the carbon layers lengthen and become more planar, interlayer spacing decreases, and the number of defects decreases (Grew, 1974; Buseck and Huang, 1985; Teichmuller, 1987).

3.4. Diamond Pseudomorphs from the Beni Bousera and Ronda Peridotite Massifs

An octahedral or cubic morphology of graphite is the most convincing evidence for graphitized diamond. Graphite pseudomorphs after diamond have been recognized in the Beni Bousera peridotite massif in northern Morocco and the Ronda peridotite massif in southern Spain (e.g., Pearson et al., 1989; Davies et al., 1993). Most graphite from both locations has

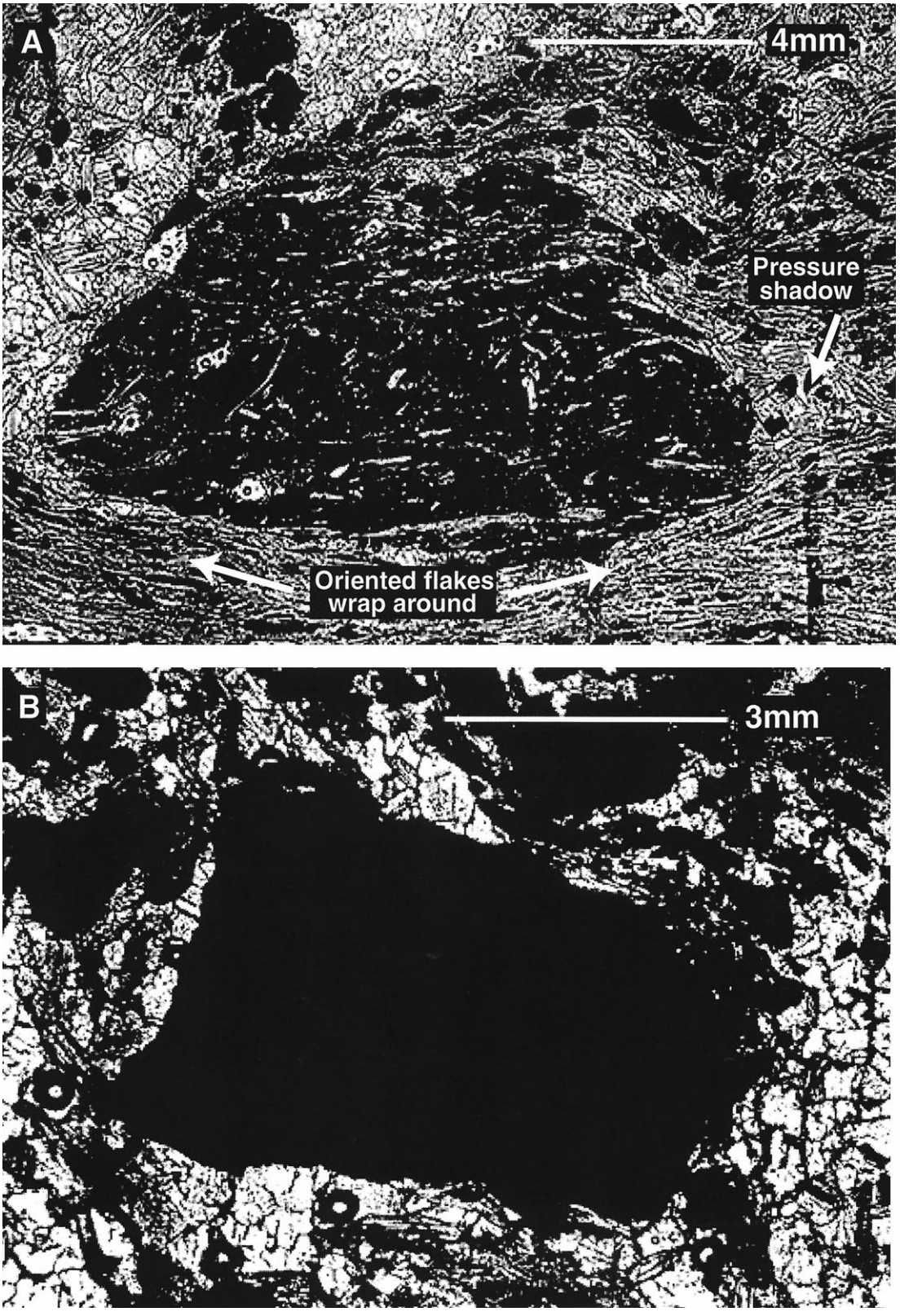

Fig. 4. Thin sections (in unpolarized light) of graphite schist from Unit #1 cut perpendicular to the foliation: (a) subangular graphite aggregate (13 × 10 mm) with phengite and rutile inclusions. The foliation is defined by graphite and phengite flakes that wrap around the graphite aggregate. Note the pressure shadows of quartz and coarse-grained phengite that have formed around the aggregate. Vertical black lines and rings of dots in lower right-hand and upper left-hand corners are from marking thin section for electron microprobe analysis; (b) cuboid graphite aggregate (about 6 mm long) typical of those in graphite schist in Unit #1.

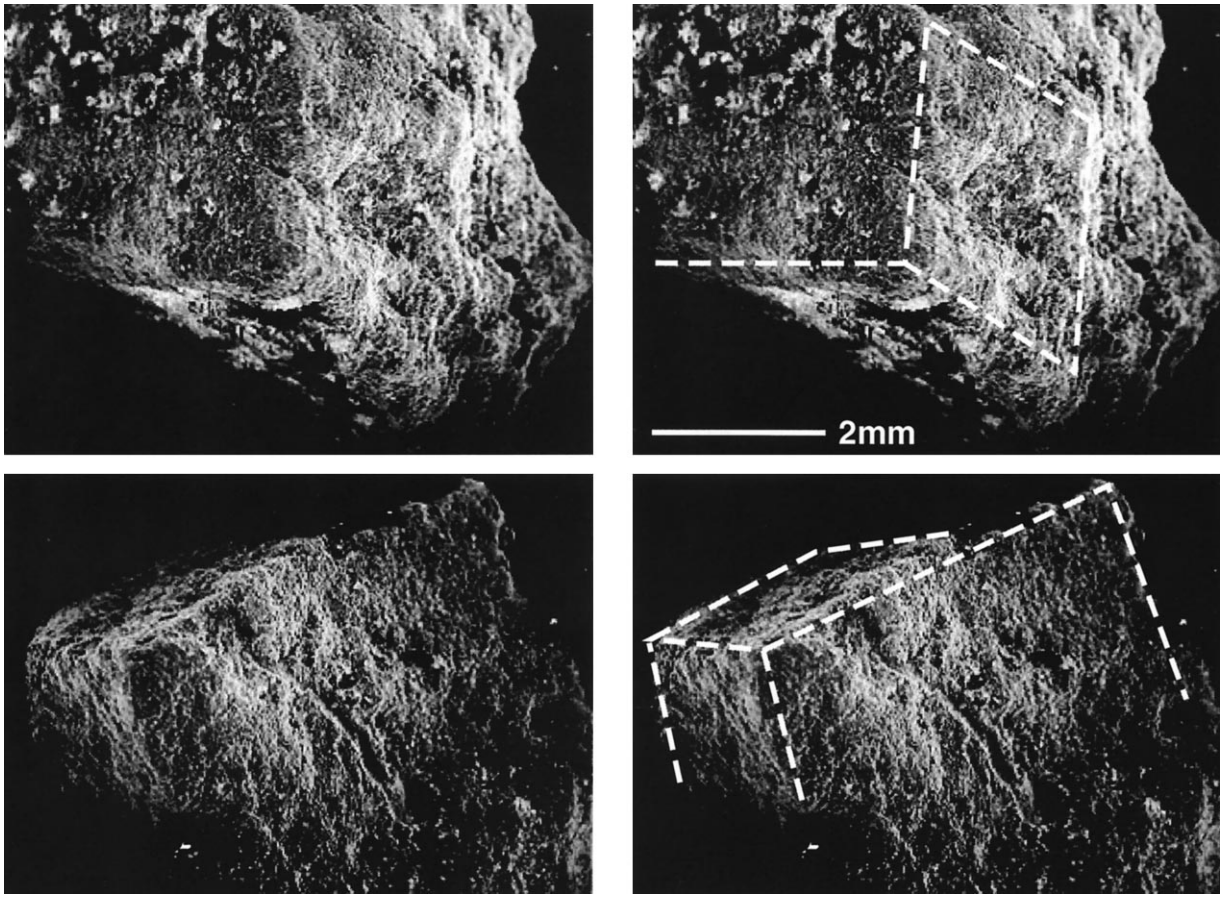

Fig. 5. SEM images showing the external morphology of graphite aggregates that display rough or perhaps slightly deformed cubic forms; dashed white lines trace the edges of cubes on the right side of the figure. These images are similar to those described by Pearson and Nixon (1996) for aggregates from the Beni Bousera massif. Aggregates have about a 4 mm edge length.

cubic symmetry, but more than 30% of the graphite occurs as aggregates with no obvious external morphology. Graphite cubes and octahedra are commonly 2–8 mm in diameter, but can be up to 12–20 mm (Pearson et al., 1989; Davies et al., 1991, 1993; Pearson and Nixon, 1996). Dissolution of silicates surrounding the graphite with hydrofluoric acid reveals graphite cubes and octahedra, but more commonly, graphite with an ovoid form which is due to a 0.01–3 mm thick fibrous graphite shell that coats most of the octahedra; crushing samples separates some of the graphite cubes and octahedra from the shell graphite (Pearson et al., 1989). Pearson and Nixon (1996) described graphite aggregates occurring as octahedra and other forms of cubic symmetry in the Beni Bousera massif. The rounded, coated graphite aggregates shown in thin section in their Fig.10a,b and in an SEM image in their Fig. 11a are strikingly similar to graphite aggregates from the Maksyutov Complex.

Diamond crystal morphology is largely controlled by the temperature and pressure conditions and/or oxygen fugacity at the time of crystallization. Octahedral diamonds result from crystallization at either lower relative temperatures and/or higher pressures, or an oxygen fugacity near magnetite-wustite (Robinson et al., 1978; Taylor, 1985; Sobolev and Shatsky, 1990; Deines et al., 1993). The morphology of the resulting graphite aggregates is most likely dictated by the original crystal form of the diamond (Pearson and Nixon, 1996).

Octahedral forms of diamond predominate in most localities worldwide (Taylor, 1985), but the entire range of morphologies from cubic to octahedral is represented in peridotite massifs (e.g., Beni Bousera), kimberlites and associated mantle xenoliths (e.g., Orapa, Botswana; Roberts Victor, South Africa; and Yakutia, Siberia), and ultrahigh-pressure metamorphic terranes (e.g., the Kokchetav Massif, Kazakhstan; the Western Gneiss region, Norway; and Dabie Shan, China) (Sobolev and Shatsky, 1990; Shatsky et al., 1991; Viljoen et al., 1991; Xu et al., 1992; Deines et al., 1993; Jerde et al., 1993; Okay, 1993; Dobrzhinetskaya et al., 1994, 1995). Most diamonds with a cubic morphology are found in rocks with an eclogitic affinity (Spetius, 1995), as is the case for the Maksyutov Complex.

4. SAMPLE SEPARATION

Three techniques were used to separate graphite from Maksyutov rock samples for both isotopic analyses and spectroscopic studies: flotation of graphite from crushed rock samples, acid dissolution of silicates surrounding graphite, and hand-picking graphite directly from the samples. For finely disseminated graphite, manual separation from dry, crushed

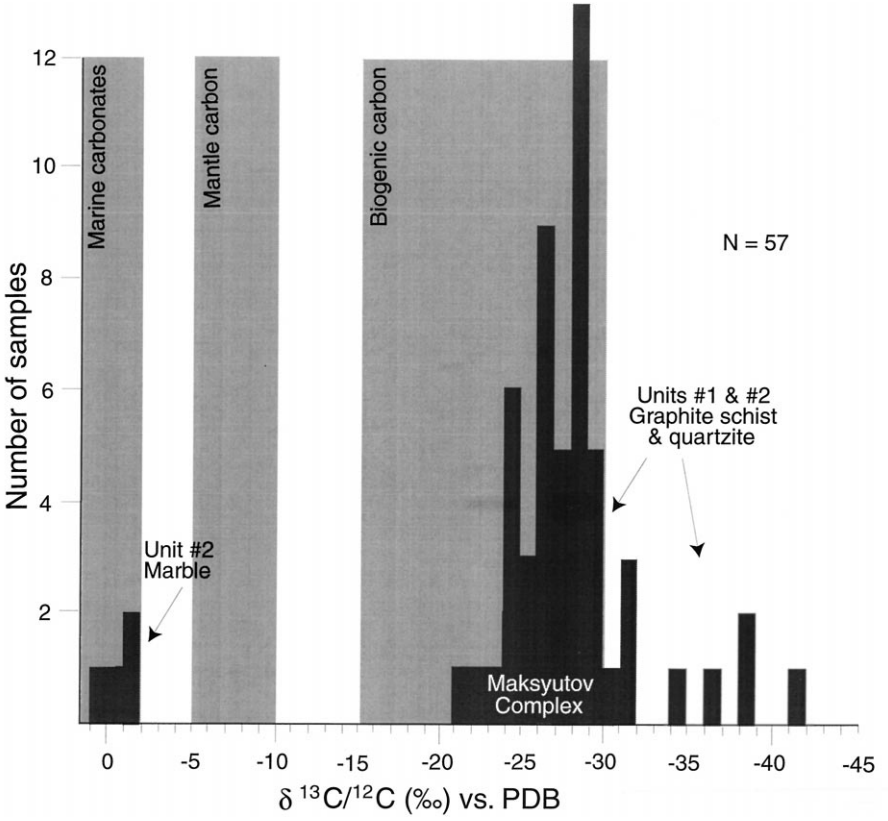

Fig. 6. Carbon isotope composition of graphite-bearing rocks and marble from the Maksyutov Complex (Table 1 contains more detailed information). Ranges of typical carbon isotope values for marine carbonates, mantle carbon, and biogenic carbon from Javoy et al. (1986).

rock was tedious, so graphite was floated in water; because of the hydrophobic character of graphite, other phases settled out and left a film of graphite on the surface of the water to be skimmed off.

Several samples, including cuboid aggregates, were dissolved in a solution of hydrofluoric and hydrochloric acid to separate graphite from the silicates, in an attempt to preserve any relict cubes or octahedra (shown in Fig. 5). A 1:1 solution of 48.8–49.2% HF and 36.5–38.0% HCl was used to dissolve the silicates surrounding the graphite aggregates in cm-sized samples. About half of the mixture was decanted every 48 h and refreshed with another 1:1 solution; this process was repeated at least five times. The procedure left some insoluble fluorides, but did not interfere with the final graphite separation by hand.

For carbon isotope analyses, graphite was hand-picked from several samples of the graphite schist. Aggregate graphite was readily separated by hand from the graphite occurring in the foliation to allow analyses of both forms.

5. CARBON ISOTOPE GEOCHEMISTRY

Carbon isotope measurements were performed at the University of California, Davis and the Geophysical Laboratory, Carnegie Institution in Washington, D. C. to establish $\delta^{13}C$ vs. PDB for graphite from the Maksyutov Complex. An elemental analyzer was used at UC Davis and samples were compared to the USGS graphite standard #24 (−16.0‰ vs. PDB), while at the Geophysical Laboratory, samples were analyzed on a mass spectrometer and compared to NBS-21 standard (−28.1‰ vs. PDB); several samples were analyzed at both facilities to provide an interlaboratory calibration. The isotopic composition of carbon is expressed in terms of delta notation (Hoefs, 1987):

$$\delta^{13}C(‰) = [(^{13}C/^{12}C)_{spl} - (^{13}C/^{12}C)_{std}]/(^{13}C/^{12}C)_{std} \times 10^3.$$

The reference standard is CO_2 gas released from belemnites of the Peedee Formation (PDB).

Comparison of these values with carbon isotope compositions for diamonds in other continent-continent collision zones, kimberlites, and peridotites with graphite pseudomorphs after diamond establishes the source of carbon in these high-grade rocks and perhaps will lead to a fuller understanding regarding carbon cycling and the geochemistry of the mantle.

Carbon isotope ratios for Unit #1 mica schist range from about −21 to −42‰, with a pronounced frequency peak around −28‰ (Fig. 6). The range of carbon isotope values for the Maksyutov Complex is comparable to that in microdiamonds from the UHP Kokchetav Massif, Kazakhstan (Sobolev et al., 1979; Sobolev and Shatsky, 1990), diamonds with eclogitic inclusions in kimberlitic rocks and associated mantle xenoliths (e.g., Milledge et al., 1983; Galimov, 1988) and

Table 1. Representative carbon isotope data for graphite

Sample	Rock type	Mass*	Peak size	$\delta^{13}C/^{12}C$
	Whole-rock graphite, Unit #1			
M-16-94	schist	10.2	N/A	-38.60
MC-67-95	quartzite	21.8	1.60E-09	-27.40
MC-192-95	quartzite	22.2	1.40E-09	-42.00
MC-105-95	quartzite	21.4	1.90E-09	-36.60
MC-203-95	blueschist†	30.2	1.60E-09	-28.50
MC-204-95	eclogite†	34.7	1.00E-09	-28.90
	Whole-rock graphite, Yumaguzinskaya sub-unit			
MC-136-95	quartzite	34.1	1.60E-09	-24.60
MC-138-95	quartzite	32.5	1.20E-09	-26.60
	Whole-rock graphite, Unit #2			
MC-220-95	metabasalt	4.6 mg	N/A	-21.17
MC-107b-95	metabasalt	2.7 mg	N/A	-25.77
MC-217b-95	quartzite	3.5 mg	N/A	-23.29
MC-219-95	quartzite	4.6 mg	N/A	-24.76
	Aggregate graphite, Unit #1			
M-16-94	schist	31.5	N/A	-29.20
	In-foliation graphite, Unit #1			
M-16-94	schist	32.3	N/A	-31.60
	Marble, Unit #2			
MK-192-95	marble	3.73 mg	N/A	0.49

$\delta^{13}C/^{12}C$ in units of per mil.
* Samples analyzed using an elemental analyzer have mass listed in μg; samples analyzed in multi-port are listed in mg.
† Graphite found as inclusions within garnet and in the matrix.

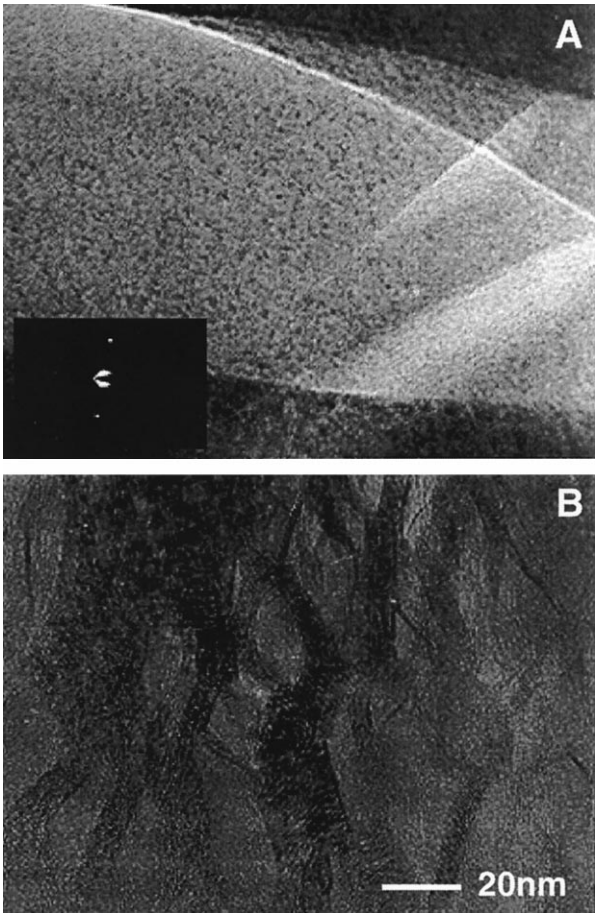

Fig. 7. TEM images of a graphite aggregate. (a) shows fairly straight lattice fringes; graphite contains many lattice fringe terminations. The inset box is a selected area diffraction pattern for the graphite. (b) shows the anastamosing character of some crystallites.

graphite pseudomorphs after diamond in the Beni Bousera peridotite massif, Morocco (Slodkevich, 1983; Pearson et al., 1989, 1995). However, kimberlitic and peridotitic diamonds have a wider range of carbon isotope values, from about +2 to −34‰, and a large frequency peak at −5 to −6‰ (Milledge, 1983; Kirkley and Gurney, 1991; Kirkley et al., 1991) indicating a mantle source for the carbon (see Mattey, 1987; Galimov, 1988).

Very negative carbon isotope values might represent carbon from a deep mantle source, perhaps a primitive mantle carbon reservoir (Javoy et al., 1986; Deines et al., 1987, 1993; Galimov, 1988), but more likely these rocks have retained their original biogenic carbon signature (Milledge et al., 1983; Kirkley et al., 1991). Javoy et al. (1986) and Mattey (1987) give ranges for various carbon sources: Organic carbon has a $\delta^{13}C$ signature ranging from about −15 to −30‰ (mean $\delta^{13}C$ = −25‰), whereas marine carbonates have a mean value around 0‰, and mantle carbon ranges from −5 to −8‰. Intermediate values in kimberlites and associated rocks probably result from the mixing of subducted biogenic carbon and mantle carbon in the uppermost mantle (Javoy et al., 1986).

In the Maksyutov Complex, there are no apparent differences in isotopic signature according to the type of graphite sampled; blocky aggregates, graphite aligned in the foliation, and inclusions in other minerals all occupy the same general isotopic range for both tectonic units. Marble is found only rarely as small blocks in Unit #2 and has a mean carbon isotope value of about −1‰ vs. PDB, which corresponds to typical marine carbonates (Table 1). Nitrogen analyses for graphite yield values which indicate atmospheric contamination.

6. SPECTROSCOPIC AND MICROSCOPIC STUDIES

Transmission electron microscopy (TEM), x-ray diffraction (XRD), and both infrared and laser Raman spectroscopic techniques were used to investigate the structure of the graphite aggregates in order to gain insight into their origin and subsequent history. Infrared spectroscopy shows whether or not relict organic compounds remain within the cuboid aggregates. X-ray diffraction characterizes a bulk sample (up to a cm-size area) which is thought to be useful in the determination of graphite crystallization state, although heterogeneity within the sample may be missed because of the scale and nature of the analysis. Sample preparation for XRD is destructive and may change the character of the graphite. Transmission electron microscope analyses are on the scale of a few Å and serve as an excellent tool for investigating the structure of the crystallites, but do not easily allow characterization of a sample as a whole. Laser

Raman microspectroscopy allows an intermediate-scale analysis of graphite crystallization in the cuboid aggregates, with a beam size on the order of about 100 μm; it is possible to run a profile across individual graphite aggregates to check for localized differences in crystallization state within a single sample.

6.1. Transmission Electron Microscopy

Transmission electron microscopy samples were prepared by epoxying a copper sample holder ring directly onto graphite aggregates, removing and mounting the aggregate into a TEM sample holder, then ion milling through the center of the aggregate. Imagery of the graphite aggregates from Maksyutov show that the graphite contains minor defects such as dislocations, causing lattice-fringe terminations (Fig. 7). Study of one graphite aggregate shows fairly straight, uniformly spaced lattice fringes containing defects such as lattice-fringe terminations and crystallites that have an anastamosing character, showing a lower degree of structural order.

Selected-area diffraction (SAD) patterns are diffuse and lack rings, which probably result from the defects seen in TEM imaging (Buseck and Huang, 1985). Low-magnification TEM images show that graphite crystals have a very roughly aligned orientation; graphite grains in reflected light appear to be aligned in two preferred directions subparallel to the external morphology of the aggregates. Induced effects from the ion milling process may explain some of the apparent defects, but are probably not responsible for all those seen in TEM images because the alleged milling effects continue into the thicker portions of the milled thin section.

6.3. X-Ray Diffraction

Samples were run employing CuK_a radiation and a Philips x-ray diffractometer. X-ray diffraction spectra were used to determine the degree of crystallinity in powdered graphite aggregates after obtaining the results of the TEM. Graphite samples were prepared for XRD analysis by mixing powder in distilled water, followed by drying, in order to orient graphite flakes with the (002) planes coincident with the specimen holder; other analyses were performed on dry, powdered graphite. The samples were scanned from 5 to 45° 2θ, scanning 0.05° 2θ every second. Sharp peaks on x-ray diffraction spectra from powdered, and oriented samples for the aggregates indicate that the graphite is well crystallized; no broad peaks were obtained, and all 2θ angles correspond with graphite d-spacings. Interplanar d_{002} spacing for the aggregates is ~3.36 Å, which is the d-spacing for fully-ordered graphite according to Warneke and Ernst (1984) and Tagiri and Oba (1986); peak width at half-height (in °2θ) is about 0.324.

6.4. Laser Raman Microspectroscopy

First-order spectra were analyzed from 1200 to 1700 cm^{-1} and second-order spectra from 2350 to 3350 cm^{-1} on a Lab-Ram spectrometer; these scans analyzed for the first-order single band at about 1582 cm^{-1} that is characteristic of well-crystallized graphite as well as two overlapping bands near 2700 cm^{-1} in second-order wave numbers (Pasteris and Wopenka, 1991). Disorder in graphite appears as a broadening

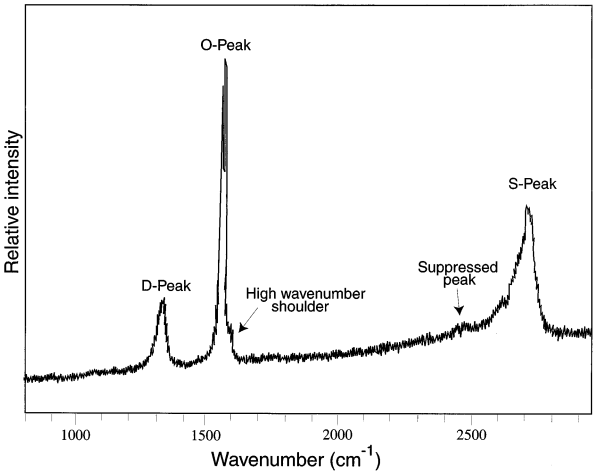

Fig. 8. Laser Raman spectra of graphite aggregates showing two large peaks, with the first-order peak at about 1582 cm^{-1} (O-peak), a peak at 1360 cm^{-1} showing disorder (D-peak), and a smaller, broad second-order peak at about 2700 cm^{-1} (S-peak). Note the high wavenumber shoulder on the O-peak and a suppressed peak at about 2450 cm^{-1}.

of the 1582 cm^{-1} band and its shift toward higher wavenumbers as a result of the development of an additional band near 1360 cm^{-1}; second-order spectra exhibit a broadening of the band at 2700 cm^{-1}, the loss of resolution of the two overlapping bands that create that peak, and the suppression of a peak at about 2450 cm^{-1} (Pasteris and Wopenka, 1991).

Most analyses of Maksyutov graphite aggregates show two large peaks, at about 1582 cm^{-1} and 1360 cm^{-1}, and a smaller, broad peak at about 2700 cm^{-1}. Figure 8 shows a peak at about 1360 cm^{-1}, a shoulder developed on the high wavenumber side of the 1582 cm^{-1} peak, and a suppressed peak at about 2450 cm^{-1} which indicate minor disorder in the graphite probably resulting from the dislocations found in TEM imaging. The Raman spectra for these aggregates are similar to those shown for graphite in the chlorite to biotite zone of Barrovian metamorphism for metapelites, according to Wopenka and Pasteris (1993).

6.5. Infrared Spectroscopy

If organic C-H or C-O bonds exist, it would follow that these graphite aggregates could never have been diamond, for organic bonds would certainly have been broken during transformation to diamond. Graphite aggregates separated by acid dissolution were analyzed with an infrared spectrometer to search for organic compounds. Graphite was powdered and mixed with KBr in the ratios 1:100 and 1:20. Each sample was scanned 500 times in addition to the standard KBr for background analyses; background KBr scans were subtracted from the graphite scans to isolate graphite peaks. The spectra show a broad hump between 2900 and 3700 cm^{-1} (Fig. 9); this adsorptance represents O-H bonds probably from water adsorbed by the sample. Two small peaks between 2300 and 2400 cm^{-1} result from atmospheric CO_2. The large, broad, composite peak between 400 and 800 cm^{-1} is from silicates that were not dissolved during the acid dissolution process and/or from

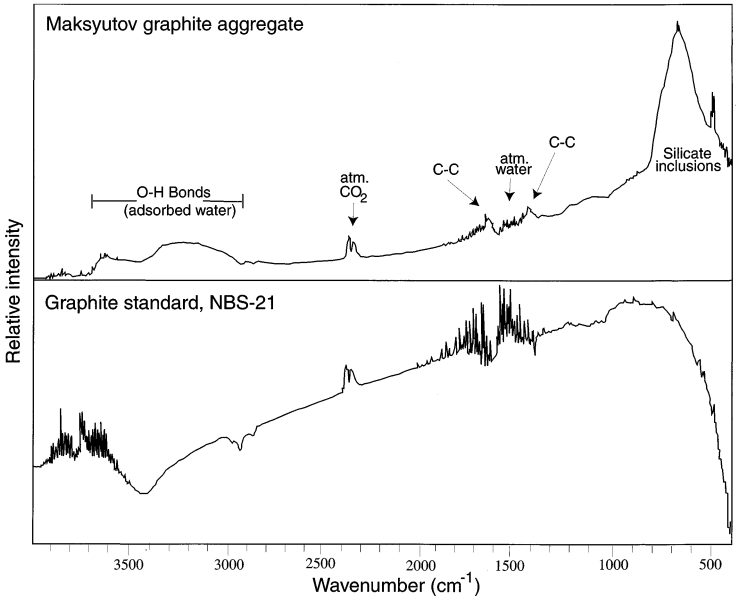

Fig. 9. Infrared spectra of acid-separated graphite aggregates. Peaks are at about 1425 cm^{-1} and about 1633 cm^{-1}, both probably representing C-C bonds.

inclusions in the graphite. Two low-intensity absorption bands were isolated in the graphite, one at about 1425 cm^{-1} and another at about 1633 cm^{-1}.

The wavenumbers associated with the two peaks described above might represent C-C bonds or C-O or C-H bonds (Robin and Rouxhet, 1978; Tissot and Welte, 1978). A USGS graphite standard (NBS-21) was run subsequent to the aggregate sample; two noisy peaks representing C-C bonds are located at approximately the same wavenumber positions as the aggregate. It is more probable that the two similar peaks are C-C bonds and not organic-group bonds.

6.6. Rate of Graphitization of Diamond

Experiments on rates of transformation from $C_{Diamond} \rightarrow C_{Graphite}$ show that graphitization per unit time can be estimated by:

$$dx/dt = C_{exp}^{-(\Delta E + P\Delta V)/RT,}$$

where C is a constant proportional to graphitization rate, ΔE is the activation energy, and ΔV is the activation volume (Davies and Evans, 1972). The low activation volume for graphitization ($\sim 10 cm^3 \bullet mol^{-1}$) indicates that the influence of pressure is small; thus the rate of graphitization is largely dependent on temperature (Pearson et al., 1995). Experimentally determined activation energies for graphitization of diamond are lowest for {110} faces of octahedra (760 $kJmol^{-1}$) and highest for {111} faces (1060 $kJmol^{-1}$) under anhydrous conditions (Pearson and Nixon, 1996). Using the activation energy for the graphitization of {110} faces, Pearson et al. (1995) calculated that the complete conversion of a diamond octahedron ($\sim$10 mm edge length) to graphite would require about 1 m.y. at 1200°C or 1 b.y. at 1000°C.

Rate studies for diamond graphitization require a much slower exhumation rate and higher temperature than is thought to have occurred in the evolution of the Maksyutov Complex. However, these dry graphitization experiments do not take into account the presence of fluids and other rate-enhancing constituents (Tagiri and Oba, 1986) that increase the kinetics of graphitization during return to the Earth's surface. Reequilibration that occurred during the exhumation history of the Maksyutov Complex evidently was sufficient for complete graphitization of any diamond that had been present. Diamond is preserved in the Kokchetav Massif under only very special conditions, chiefly as armored micro-inclusions in garnet and zircon, which acted as pressure vessels (Sobolev and Shatsky, 1990; Sobolev et al., 1994).

The rate of transformation for silicates is faster than for diamond $\rightarrow$ graphite. According to Poirier (1981), the activation energy for the olivine $\rightarrow$ spinel transition is 259 $kJmol^{-1}$, which is similar to the coesite $\rightarrow$ quartz reaction (Mosenfelder and Bohlen, 1997). The correspondence of these activation energies probably reflects the reactions being controlled by diffusion of Si across an interface, which is likely to be analogous in many silicate structures (J. L. Mosenfelder, pers. commun., 1997). Therefore, if diamond has been completely back-reacted to graphite, the possibility that coesite has survived becomes very unlikely.

7. DISCUSSION

According to the results of graphite deformation experiments, deformation would be incapable of producing the cuboid morphologies seen in Maksyutov graphite aggregates. Cross-sections of graphite aggregates from Maksyutov in thin sections taken perpendicular to the foliation show a subangular, cubic morphology (Fig. 4), and display prominent pressure shadows, indicative of significant strength during deformation and recrystallization. Although SEM imagery was limited by the large size of the aggregates, rounded, or perhaps slightly

deformed cubic forms seem probable (Fig. 5). These images are very similar to thin sections and SEM images described by Pearson and Nixon (1996) of graphite pseudomorphs from the Beni Bousera massif. However, Maksyutov graphite has undergone a far more complex history of metamorphism and deformation than Beni Bousera, which probably affected the cuboid graphite morphology: Maksyutov graphite therefore only preserves cubic to rounded morphologies with no apparent difference between the form of the core and coating graphite. Graphitization of the inferred diamond precursor occurred syn- or post-deformation because of the pressure shadows that formed around some aggregates (Fig. 4a). In fact, the rounded graphite shape probably results more from the original diamond form than the deformational history that these rocks underwent.

Grew (1974) noted that XRD analysis provides no evidence for the presence of more than one type of carbonaceous material in a sample; TEM images commonly show considerable structural variability within a single grain and between different graphite grains in a single sample (Buseck and Huang, 1985). X-ray diffraction, laser Raman microspectroscopy, and TEM should all be in fairly good agreement in determining the structural order of graphite; apparent discrepancies between different techniques are simply a result of the nature of the analyses. With respect to all three techniques, graphite aggregates from the Maksyutov Complex are composed of well-crystallized graphite with minor disorder probably brought on by crystallographic defects such as dislocations.

There is no evidence for the survival of relict diamond at Maksyutov using any of these techniques. Graphite that is not pseudomorphic after diamond occurs with diamond in kimberlites and associated eclogite xenoliths, and in several other UHP terranes. If metamorphism took place near the equilibrium P-T field boundary between graphite and diamond, not all graphite may have initially transformed to diamond.

Existing experimental data on graphitization of diamond do not adequately replicate the conditions of natural rocks being exhumed from great depth and thus cannot be applied realistically to the Maksyutov Complex. Experiments using diamond in conditions duplicating those of the natural rock and under appropriate P-T and fluid-present conditions are certainly necessary to address the rate problem.

8. CONCLUSIONS

Carbon isotope ratios for graphite in Units #1 and #2 of the Maksyutov Complex indicate that it is biogenic carbon, except for graphite in marble which retains a marine carbonate signature. The morphology of the cuboid graphite aggregates is probably an original growth feature; it is not a result of deformation, as indicated by the results of graphite deformation experiments of other workers. Spectroscopic studies including TEM imaging and XRD and laser Raman microspectroscopy demonstrate that the graphite is well-crystallized with only minor dislocation defects; infrared spectroscopy shows an absence of relict organic compounds in the aggregates. Comparison of thin sections through cuboid graphite aggregates and SEM imagery of Maksyutov graphite aggregates with diamond pseudomorphs from the Beni Bousera peridotite massif shows many similarities. Maksyutov rocks have undergone a far more complicated metamorphic and deformational history and, therefore, preserve only deformed cubic to rounded forms and not the core/coating graphite relationship found in the unambiguous diamond pseudomorphs from Beni Bousera. Experimental data on diamond graphitization rates do not bear on the possibility that cuboid graphite aggregates represent pseudomorphs after diamond.

The problem of identifying the origin of these oddly shaped graphite aggregates may be unsolvable. We have tried several analytical techniques to explain the unusual character of graphite in the Maksyutov rocks, but nothing can be proven conclusively. A more thorough search of thick sections of Maksyutov eclogite and host rocks that may reveal coesite, coesite pseudomorphs, or diamond relicts is underway, but so far none has been found to substantiate earlier claims by Russian workers. This study of cuboid graphite aggregates from the Maksyutov Complex has yielded suggestive though nondefinitive results, but we believe that the preponderance of evidence supports the possibility that they are diamond pseudomorphs.

Acknowledgments—We thank Howie Spero and Douglas Rumble for help analyzing the carbon isotopes presented here, Michael Dalla Torre for aid in interpreting TEM images and XRD and infrared spectra, and Robert Jones for help operating the XRD. Special thanks are also due to the late Tracy Tingle for encouragement and support of this research. Partial funding for research in the Maksyutov Complex was derived from an NSF grant to R. G. Coleman (EAR 93-04480), a GSA Research grant to M. L. Leech (#6075-97), and McGee and Shell Fund grants from Stanford University (Mary L. Leech). This report was materially improved from very helpful and thorough reviews by Peter Buseck and Edward Grew.

REFERENCES

Armstrong L. F. (1982) Metamorphic mineral parageneses in Mesozoic and Paleogene rocks, southern east-west Cross-Island Highway, Taiwan. Master's thesis, Univ. California at Los Angeles.

Beane R. J. (1997) Petrologic evolution and geochronologic constraints for high-pressure metamorphism in the Maksyutov Complex, south Ural Mountains. Ph.D. dissertation, Stanford Univ.

Beane R. J., Liou J. G., Coleman R. G., and Leech M. L. (1995) Mineral assemblages and retrograde P-T path for high- to ultrahigh-pressure metamorphism in the lower unit of the Maksyutov Complex, Southern Ural Mountains, Russia. *Island Arc* **4,** 254–266.

Bohlen S. R. and Boettcher A. L. (1982) The quartz ↔ coesite transformation; a precise determination and the effects of other components. *J. Geophys. Res.* **87,** 7073–7078.

Buseck P. R. and Huang B.-J. (1985) Conversion of carbonaceous material to graphite during metamorphism. *Geochim. Cosmochim. Acta* **49,** 2003–2016.

Chesnokov B. V. and Popov V. A. (1965) Increasing volume of quartz grains in eclogites of the South Urals. *Dokl. Akad. Nauk SSSR* **162,** 176–178.

Dalla Torre M. et al. (1996) Very low-temperature metamorphism of shales from the Diablo Range, Franciscan Complex, California: New constraints on the exhumation path. *Geol. Soc. Amer. Bull.* **108,** 578–601.

Dalla Torre M., Ferreiro-Mahlmann R., and Ernst W. G. (1997) Experimental study on the pressure dependence of vitrinite maturation. *Geochim. Cosmochim. Acta* **61,** 2921–2928.

Davies G. and Evans T. (1972) Graphitization of diamond at zero pressure and at a high pressure. *Proc. Roy. Soc. London* **328,** 413–427.

Davies G. R., Nixon P. H., Pearson D. G., and Obata M. (1991) Graphitised diamonds from the Ronda peridotite massif, S. Spain. *Proc. 5th Intl. Kimberlite Conf.,* 318–326.

Davies G. R., Nixon P. H., Pearson D. G., and Obata M. (1993) Tectonic implications of graphitized diamonds from the Ronda peridotite massif, southern Spain. *Geology* **21,** 471–474.

Deines P., Harris J. W., and Gurney J. J. (1987) Carbon isotopic composition, nitrogen content and inclusion composition of dia-

monds from the Roberts Victor kimberlite, South Africa: Evidence for ^{13}C depletion in the mantle. *Geochim. Cosmochim. Acta* **51,** 1227–1243.

Deines P., Harris J. W., and Gurney J. J. (1993) Depth-related carbon isotope and nitrogen concentration variability in the mantle below the Orapa kimberlite, Botswana, Africa. *Geochim. Cosmochim. Acta* **57,** 2781–2796.

Diessel C. F. K., Brothers R. N., and Black P. M. (1978) Coalification and graphitization in high-pressure schists in New Caledonia. *Contrib. Mineral. Petrol.* **68,** 63–78.

Dobretsov N. L. and Dobretsova L. V. (1988) New mineralogic data on the Maksyutovo eclogite-glaucophane schist complex, southern Urals. *Dokl. Akad. Nauk SSSR* **300,** 111–116.

Dobretsov N. L et al. (1996) Tectonic setting and petrology of ultrahigh-pressure metamorphic rocks in the Maksyutov Complex, Ural Mountains, Russia. *Intl. Geol. Rev.* **38,** 136–160.

Dobrzhinetskaya L. F., Braun T. V., Sheshkel G. G., and Podkuiko Y. A. (1994) Geology and structure of diamond-bearing rocks of the Kokchetav massif (Kazakhstan). *Tectonophysics* **233,** 293–313.

Dobrzhinetskaya L. F. et al. (1995) Microdiamond in high-grade metamorphic rocks of the Western Gneiss region, Norway. *Geology* **23,** 597–600.

Edmond J. M. and Paterson M. S. (1971) Strength of solid pressure media and implications for high pressure apparatus. *Contrib. Mineral. Petrol.* **30,** 141–160.

Edmond J. M. and Paterson M. S. (1972) Volume changes during the deformation of rocks at high pressures. *Intl. J. Rock Mech. Mineral Sci.* **9,** 161–182.

Galimov E. M. (1988) Carbon geochemistry. *Geochem. Intl.* **25,** 94–110.

Grew E. S. (1974) Carbonaceous material in some metamorphic rocks of New England and other areas. *J. Geology* **82,** 50–73.

Hoefs J. (1987) *Stable Isotope Geochemistry*. Springer-Verlag.

Holland T. J. B. (1980) The reaction albite = jadeite + quartz determined experimentally in the range 600–1200 degrees C. *Amer. Mineral.* **65,** 129–134.

Javoy M., Pineau F., and Delorme H. (1986) Carbon and nitrogen isotopes in the mantle. *Chem. Geol.* **57,** 41–62.

Jerde E. A., Taylor L. A., Crozaz G., Sobolev N. V., and Sobolev V. N. (1993) Diamondiferous eclogites from Yakutia, Siberia: Evidence for a diversity of protoliths. *Contrib. Mineral. Petrol.* **114,** 189–202.

Kennedy C. S. and Kennedy G. C. (1976) The equilibrium boundary between graphite and diamond. *J. Geophys. Res.* **81,** 2467–2470.

Kirkley M. B. and Gurney J. J. (1991) Carbon isotope modelling of biogenic origins for carbon in eclogitic diamonds (abstr.). *Extended Abstr. 5th Intl. Kimberlite Conf.*, 40–43.

Kirkley M. B., Gurney J. J., Otter M. L., Hill S. J., and Daniels L. R. (1991) The application of C isotope measurements to the identification of the sources of carbon in diamonds: A review. *Appl. Geochem.* **6,** 477–494.

Kretz R. (1996) Graphite deformation in marble and mylonitic marble, Grenville Province, Canadian Shield. *J. Meta. Geol.* **14, 399–412.**

Landis C. A. (1971) Graphitization of dispersed carbonaceous material in metamorphic rocks. *Contrib. Mineral. Petrol.* **30,** 34–45.

Lennykh V. I., Valizer P. M., Beane R. J., Leech M. L., and Ernst W. G. (1995) Petrotectonic evolution of the Maksyutov Complex, south Urals, Russia: Implications for ultrahigh-pressure metamorphism. *Intl. Geol. Rev.* **37,** 584–600.

Matte P., Maluski H., Caby R., Nicholas A., Kepezhinkskas P., and Sobolev S. (1993) Geodynamic model and $^{39}Ar/^{40}Ar$ dating for the generation and emplacement of the high pressure metamorphic rocks in SW Urals. *C. R. Acad. Sci. Paris* **317,** 1667–1674.

Mattey D. P. (1987) Carbon isotopes in the mantle. *Terra Cognita* **7,** 31–37.

Milledge H. J., Mendelssohn M. J., Seal M., Rouse J. E., Swart P. K., and Pillinger P. T. (1983) Carbon isotope variation in spectral type II diamonds. *Nature* **303,** 791–792.

Mosenfelder J. L. and Bohlen S. R. (1997) Kinetics of the coesite to quartz transformation. *Earth Planet. Sci. Lett.* **153,** 133–147.

Okay A. I. (1993) Petrology of a diamond and coesite-bearing metamorphic terrain: Dabie Shan, China *Eur. J. Mineral.* **5,** 659–675.

Pasteris J. D. and Wopenka B. (1991) Raman spectra of graphite as indicators of degree of metamorphism. *Canadian Mineral.* **29,** 1–9.

Pearson D. G. and Nixon P. H. (1996) Diamonds in young orogenic belts: graphitised diamond from Beni Bousera, N. Morocco, a comparison with kimberlite-derived diamond occurrences and implications for diamond genesis and exploration. *Africa Geosci. Rev.* **3,** 295–316.

Pearson D. G., Davies G. R., and Nixon P. H. (1989) Graphitized diamonds from a peridotite massif in Morocco and implications for anomalous diamond occurrences. *Nature* **338,** 60–62.

Pearson D. G., Davies G. R., and Nixon P. H. (1995) Orogenic ultramafic rocks of UHP (diamond facies) origin. In *Ultrahigh Pressure Metamorphism* (ed. R. G. Coleman and X. Wang), pp. 456–510. Cambridge Univ. Press.

Poirier J. P. (1981) On the kinetics of olivine-spinel transition. *Phys. Earth Planet. Int.* **26,** 179–187.

Powell R. (1985) Regression diagnostics and robust regression in geothermometer/geobarometer calibration: the garnet-clinopyroxene geothermometer revisited. *J. Metam. Geol.* **3,** 231–243.

Robin P. L. and Rouxhet P. G. (1978) Characterization of kerogens and study of their evolution by infrared spectroscopy: Carbonyl and carboxyl groups. *Geochim. Cosmochim. Acta* **42,** 1341–1349.

Robinson D. N., Gurney J. J., and Shee S. R. (1978) Diamond eclogite and graphite eclogite xenoliths from Orapa, Botswana In *Kimberlites. II. The Mantle and Crust-Mantle Relationships* (ed. J. Kornprobst), pp. 11–24. Elsevier Sci. Publ.

Ross J. V. and Bustin R. M. (1990) The role of strain energy in creep graphitization of anthracite. *Nature* **343,** 58–60.

Ross J. V., Bustin R. M., and Rouzaud J. N. (1991) Graphitization of high rank coals the role of shear stain: experimental considerations. *Organic Geochemistry* **17,** 585–596.

Shatsky V. S., Sobolev N. V., and Yefimova E. S. (1991) Morphological features of accessory microdiamonds from metamorphic rocks of the Earth's crust. *Ext. Abstr. 5th Intl. Kimberlite Conf.*, 94–94. (abstr.).

Slodkevich V. V. (1983) Graphite pseudomorphs after diamond. *Intl. Geol. Rev.* **25,** 497–514.

Sobolev N. V. and Shatsky V. S. (1990) Diamond inclusions in garnets from metamorphic rocks. *Nature* **343,** 742–746.

Sobolev N. V., Galimov E. M., Ivanovskaya I. N., and Efimova E. S. (1979) Isotopic composition of carbon from diamonds containing crystalline inclusions. *Dokl. Akad. Nauk SSSR* **249,** 1217–1220 (in Russian).

Sobolev N. V., Shatsky V. S., Valivov M. A., and Goryainov S. V. (1994) Zircon from ultra high pressure metamorphic rocks of folded regions as an unique container of inclusions of diamond, coesite, and coexisting minerals. *Dokl. Akad. Nauk* **334,** 488–492 (in Russian).

Sobolev V. S. and Sobolev N. V. (1980) New proof on very deep subsidence of eclogitized crustal rocks. *Dokl. Akad. Nauk SSSR* **250,** 88–90.

Spetius Z. V. (1995) Occurrence of diamond in the mantle: A case study from the Siberian Platform. *J. Geochem. Explor.* **53,** 25–39.

Tagiri M. and Oba T. (1986) Hydrothermal syntheses of graphite from bituminous coal at 0.5–5 kbar water vapor pressure and 300–600°C. *J. Japan. Assoc. Mineral. Petrol. Econ. Geol.* **81,** 260–271.

Taylor W. R. (1985) A reappraisal of the nature of fluids included by diamond—a window to deep-seated mantle fluids and redox conditions. In *Stable Isotopes and Fluid Processes in Mineralization* (ed. H. K. Herbert and S. E. Ho), pp. 333–349. Univ. Western Australia Pub 23.

Teichmuller M. (1987) Organic material and very low-grade metamorphism. In *Low Temperature Metamorphism* (ed. M. Frey), pp. 114–161. Blackie.

Tissot B. P. and Welte D. H., ed. (1978*) Petroleum Formation and Occurrence: A New Approach to Oil and Gas Exploration.* Springer-Verlag.

Viljoen K. S. et al. (1991) Diamond- and graphite-bearing peridotite xenoliths from the Roberts Victor kimberlite, South Africa. *Proc. 5th Intl. Kimberlite Conf.*, 318–326.

Warneke L. A. and Ernst W. G. (1984) Progressive Cenozoic metamorphism of rocks cropping out along the southern east-west Cross-Island Highway, Taiwan. *Mem. Geol. Soc. Amer.* **6,** 105–132.

Wopenka B. and Pasteris J. D. (1993) Structural characterization of kerogens to granulite-facies graphite: Applicability of Raman microprobe spectroscopy. *Amer. Mineral.* **78,** 533–557.

Xu S. et al. (1992) Diamond from the Dabie Shan metamorphic rocks and its implication for tectonic setting. *Science* **256,** 80–82.

Zonenshain L. P., Kuzmin M. I., and Natavov L. M. (1990*) Geology of the USSR: A Plate Tectonic Synthesis. AGU Geodyn. Ser. 21.*